Rev. Roum. Sci. Techn.– Électrotechn. et Énerg.
Vol. **68**, *4*, pp. 331–338, Bucarest, 2023

DIRECT TORQUE CONTROL SCHEME FOR LESS HARMONIC CURRENTS AND TORQUE RIPPLES FOR DUAL STAR INDUCTION MOTOR

SIFELISLAM GUEDIDA[1], BEKHEIRA TABBACHE[1], KAMAL NOUNOU[1], MOHAMED BENBOUZID [2]

Keywords: Direct torque control (DTC); 3 and 5-level torque regulators; Harmonic currents; Torque ripples; Steady-state error torque; Dual star induction motor (DSIM).

Multi-phase machine drives are widely used in high-power applications such as naval propulsion and railway traction. In the control context, direct torque control (DTC), based on the large voltage vectors, is the most used control for a dual-star induction motor. However, these techniques suffer from steady-state errors and torque ripples. Therefore, the stator phase currents have a non-sinusoidal waveform, which leads to high losses and reduces the drive efficiency of the system caused by considerable harmonic currents. This paper presents a modified direct torque control (MDTC) based on two steps to select the appropriate vector to supply the dual star induction motor (DSIM) and effectively reduce the harmonic currents. Moreover, this paper deals with a comparative study of 3-level, 5-level, and modified 5-level torque regulators to reduce the steady-state error and torque ripple. In addition, a PI controller is incorporated for the modified five-level torque regulator to reduce the torque error at low, medium, and high speeds. Moreover, an investigation of switching and core losses has been done for the DSIM drive. Finally, validation results have been presented to prove the effectiveness of developed direct torque control of the dual star induction motor (DSIM) under different operating conditions.

1. INTRODUCTION

Recently, multiphase machines have been more advantageous than three-phase machines, especially for high-power applications regarding reliability, elimination of space harmonics, and minimization of torque ripples and rotor losses [1]. In industry applications, dual star induction motors, with two three-phase windings shifted by 30 degrees, are one of the most widely used multiphase machines due to eliminating the sixth harmonic torque pulsation [2–5]. However, the strong coupling between torque and flux in the dual-star induction motor further complicates its control [6–8]. For this reason, several techniques based on indirect field-oriented control (IFOC) to separate flux and torque [5, 9–10] are widely discussed in the literature. However, these techniques suffer from the variation of the induction motor parameters. Hence, direct torque control techniques are an alternative solution for driving three-phase motors due to their advantages, particularly the fast dynamic torque response and the stable flux control over all speed ranges [8, 11–12]. Direct torque control is also applied to the dual-star induction motor [13–16]. For this, the six-leg inverter is used to supply the motor (DSIM). It contains sixty-four (64) voltage vectors to offer several possibilities for DTC techniques [3, 17]. In this context, direct torque control, based on the large vector voltage, applied to dual start induction motor suffers from harmonic stator currents, especially the harmonic components in the (*x*-*y*) subspace according to vector space decomposition (VSD) [3, 17–21]. This classical direct torque control is based on a two and three-level hysteresis controller to control the stator flux amplitude and electromagnetic torque, respectively. However, the used hysteresis controllers provide undesirable torque, stator flux ripples, and steady-state error of torque [15].

In this context, this paper proposes a modified direct torque control to minimize the harmonics of the stator current and reduce ripples and steady-state error of torque [22–33]. It is based on two steps to select the appropriate vectors to supply the dual star induction motor (DSIM), effectively reducing the harmonic currents. In addition, the hysteresis controllers of the electrometric torque are instead by a developed 5-level regulator based on more vector voltages to reduce the torque ripples and the error torque [26, 30, 32]. In low, medium, and high speed, a PI controller is incorporated to the 5-level regulator to in improve the torque response.

Finally, validation results are performed to demonstrate the effectiveness of the developed direct torque control applied the dual star induction motor (DSIM) under the different operating conditions. Moreover, a comparative investigation has been carried out in this paper.

2. DTC OF DUAL STAR INDUCTION MOTOR (DSIM)

2.1. DSIM MODEL

The dual star induction motor (DSIM) is supplied by a six-leg voltage inverter (Fig. 1). According to the vector space decomposition (VSD) approach (the electrical model, magnetic and mechanical equations), the DSIM in Fig. 1, can be decoupled into three simple independent subspaces, which are (α-β), (*x*-*y*) and (o_1-o_2) subspaces [3].

The total electromagnetic conversion is carried out in the (α-β) subspace. The (*x*-*y*) subspace creates the harmonic currents of order k=6m±1 (m=1, 3, 5...). In the (o_1-o_2) subspace the zero sequence components are set to zero in the isolated neutral points.

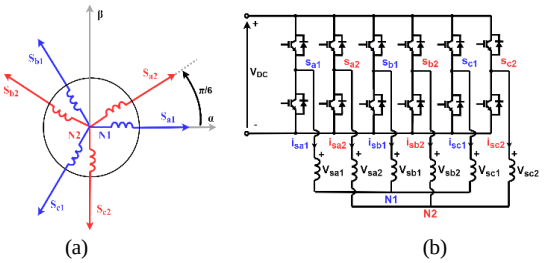

(a) (b)

Fig. 1 – Representation of dual star induction motor and power inverter: a) windings of the DSIM; b) voltage source inverter fed DSIM.

[1]UER ELT, École Militaire Polytechnique, 16111 Algiers, Algeria, E-mails: d_guedida.sifelislam@emp.mdn.dz, bekheira.tabbache@emp.mdn.dz, kamel.nounou@emp.mdn.dz
[2]UMR CNRS 6027 IRDL, University of Brest, 29238 Brest, France, E-mail: Mohamed.Benbouzid@univ-brest.fr

DOI: 10.59277/RRST-EE.2023.68.4.2

According to the VSD approach [3], the final model of the dual star induction motor (DSIM) can be described in terms of voltage, current, and flux as follows:

$$V_{s\alpha\beta} = R_s I_{s\alpha\beta} + \frac{d\varphi_{s\alpha\beta}}{dt}, \quad (1)$$

$$V_{r\alpha\beta} = 0 = R_r I_{r\alpha\beta} + \frac{d\varphi_{r\alpha\beta}}{dt} \pm \omega\, \varphi_{r\alpha\beta}, \quad (2)$$

$$\begin{bmatrix}\varphi_{s\alpha\beta}\\ \varphi_{r\alpha\beta}\end{bmatrix} = \begin{bmatrix}L_s & M\\ M & L_r\end{bmatrix}\begin{bmatrix}I_{s\alpha\beta}\\ I_{r\alpha\beta}\end{bmatrix}, \quad (3)$$

$$V_{sxy} = R_s I_{sxy} + \frac{d\varphi_{sxy}}{dt}, \quad (4)$$

$$\varphi_{sxy} = L_{ls} I_{sxy}, \quad (5)$$

$$T_e = \frac{3}{2} p\, Im(\bar{\varphi}_s * \bar{I}_s) = p\left(\varphi_{s\alpha} I_{s\beta} - \varphi_{s\beta} I_{s\alpha}\right), \quad (6)$$

where: $V_{s\alpha\beta}$, $\varphi_{s\alpha\beta}$, $\varphi_{r\alpha\beta}$, $I_{s\alpha\beta}$– stator voltage, stator flux, rotor flux, and stator current vectors in (α-β) subspace; V_{sxy}, φ_{sxy}, I_{sxy}– stator voltage, flux, and current vectors in (*x*-*y*) subspace; R_s, L_s, L_{ls} stator resistance, inductance, and leakage self-inductance; θ_r, T_e – electrical rotor angle and electromagnetic torque.

As mentioned in eq. (6), the produced electromagnetic torque of the dual star induction motor (DSIM) in the subspace (α-β) is like that delivered by the three-phase machine [8, 11–12].

2.2 DIRECT TORQUE CONTROL (DTC) BASED ON LARGE VOLTAGE VECTORS

The six power legs can generate sixty-four (64) voltage vectors to supply the DSIM. The voltage vectors in the subspace (α-β) and (*x*-*y*) can be shown in Fig. 2. The active voltage vectors in the subspace (α-β) can grouped into four dodecagons (D_1, D_2, D_3, and D_4). Their amplitude has been given as follows [3, 33]:

$$\begin{cases} V_{D4} = V_{max} = 2\frac{2}{3}V_{dc}\cos 15^0 = \frac{\sqrt{6}+\sqrt{2}}{3}V_{dc} \\ V_{D3} = V_{mid1} = 2\frac{2}{3}V_{dc}\cos 45^0 = \frac{2}{3}\sqrt{2}V_{dc} \\ V_{D2} = V_{mid2} = \frac{2}{3}V_{dc} \\ V_{D1} = V_{min} = 2\frac{2}{3}V_{dc}\cos 75^0 = \frac{\sqrt{6}-\sqrt{2}}{3}V_{dc} \end{cases}, \quad (7)$$

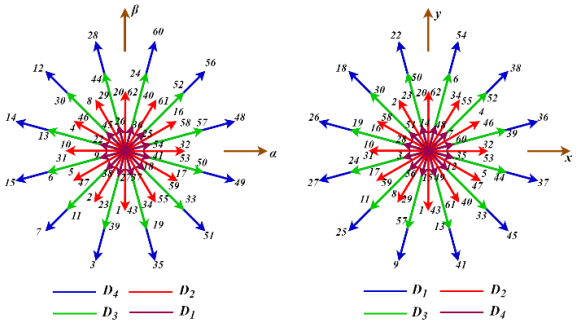

(a) (b)

Fig. 2 – Voltage space vectors generated by the power inverter: a) (α-β) sub-space; b) (*x*-*y*) sub-space.

The classical DTC of the dual-star induction motor is like that of the three-phase motor. It depends on the output of the hysteresis controllers and the switching table [15]. However, in the DTC of the DSIM, twelve (12) voltage vectors can used for each sampling time, as shown in Fig. 3. When the stator flux position is in a k-sector, the application of the appropriate voltage vector allows the instantaneous control of the flux and torque (Table 1).

Table 1

Switching table for DTC

φ_s in sector *k*		Torque (ΔT_e)		
		1	–1	0
Flux ($\Delta\varphi_s$)	1	V_{k+2}	V_{k-3}	V_{zero}
	–1	V_{k+3}	V_{k-4}	V_{zero}

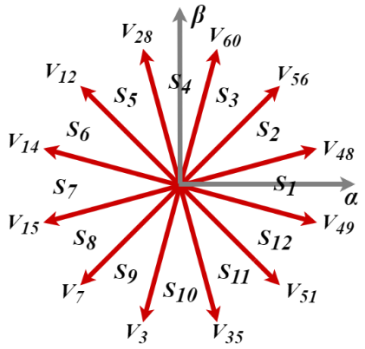

Fig. 3 – Representation of 12 sectors in (α-β) sub-space.

The classical DTC is based on the large vectors of the dodecagon (D4) in the subspace (α-β) to maximize the power.

As mentioned in Table 1, the choice of the appropriate voltage vectors to control torque and stator flux depends on the error generated by the hysteresis controllers, which are defined as follows:

$$\Delta T_e = \begin{cases} 1, & \text{to increase } T_e \\ 0, & \text{to keep } T_e \\ -1, & \text{to decrease } T_e \end{cases}, \quad (8)$$

$$\Delta\varphi_s = \begin{cases} 1, & \text{to increase } \varphi_s \\ -1, & \text{to decrease } \varphi_s \end{cases}, \quad (9)$$

The classical DTC of the dual star induction motor treats only the requirements of flux and torque in the subspace (α-β). However, the circulating currents that appear in the subspace (*x*-*y*) according to eqs. (4) and (5) are not considered.

3. DTC FOR LESS CURRENT HARMONICS

As mentioned in equations (4 and 5) in the (x-y) subspace, there is a proportional relationship between the flux and the harmonic current. Therefore, minimizing the stator flux in the (*x*-*y*) subspace reduces the circulating current in the DSIM [34–37].

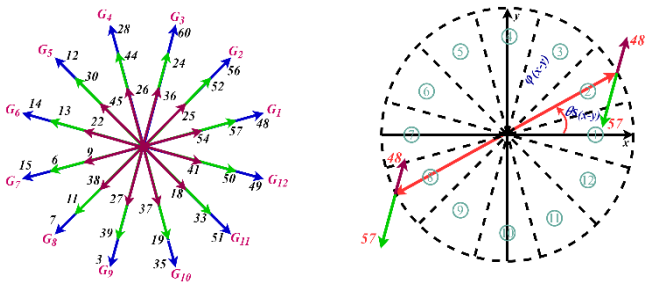

(a) (b)

Fig. 4 – Voltage vectors selected in the two subspaces: a) voltage vectors groups in sub-space (α-β); b) effects of two voltage vectors 48 and 57 in sub-space (*x*-*y*).

As shown in Fig. 4 a, twelve (12) groups can be

distinguished in the (α-β) subspace. Each group consists of three voltage vectors (V_{max}, V_{mid1}, and V_{min}) in the same direction, but in the (*x*-*y*) subspace have different effects. For example, Fig. 4 b shows that the voltage vectors V_{48} and V_{54} have the same effect in the (*x*-*y*) subspace, while the V_{57} has the opposite effect. Therefore, vector V_{57} can greatly reduce the magnitude of the flux in the (*x*-*y*) subspace and then decrease the currents [34,35].

The block diagram of the developed DTC is shown in Fig. 5. The first step is like the vector selection of the classical DTC. Moreover, the selected group depends on the hysteresis controllers' output and the stator flux's position in the (α-β) subspace. In the second step, the applied voltage vector is chosen according to the selected group and the stator flux position in the (*x*-*y*) subspace. For example, Fig. 4a shows the applied vectors are in group 1 of vectors. In this case, if the stator flux is in sectors 2 and 8, the selected voltage vectors to minimize the flux are V_{57} and V_{48}, respectively. Hence, the developed DTC can choose the appropriate voltage vectors to give a good dynamic performance for dual star induction motors (DSIM).

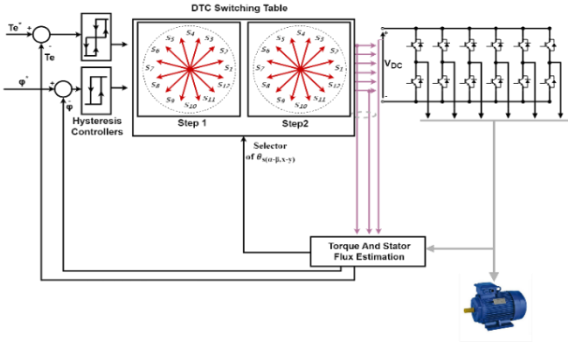

Fig. 5 – Block diagram of the proposed DTC.

4. DTC BASED ON A MODIFIED 5-LEVEL TORQUE REGULATOR

Using a three-level hysteresis regulator in the above-developed DTC causes higher torque ripples. The high number of voltage vectors (64 vectors of the six-leg inverter) can be employed to increase the levels of torque hysteresis controllers and, therefore, minimize the current harmonics. In this context, the developed DTC adopts a two-level flux regulator and a 5-level torque regulator, in which the selection of the appropriate voltage vectors requires large vectors (V_{max}), medium vectors (V_{mid1}), small vectors (V_{min}), and null vectors. These vectors meet the requirement of a stator flux regulator.

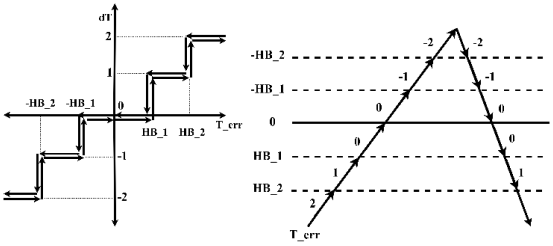

Fig. 6 – Classical 5-level torque hysteresis regulator.

Figure 6 shows that the torque error can exist in the positive or negative sides of the 5-level torque hysteresis controller when the null vectors are applied if the error is between (–HB1) and (HB1). The small vector (V_{min}) and medium vector (V_{mid1}) of voltage are used in the inner band when the torque error between (HB1 and HB2 or –HB1 and –HB2) to obtain a slow dynamic response and average torque ripples. If the torque error is on the outside, *i.e*., greater than (HB2) or less than (–HB2), the medium vector (V_{mid1}) and large vector (V_{max}) are used for fast torque and high torque ripples [37].

On the other hand, modifying the symmetry of the classical 5-level regulator is necessary to reduce the steady-state torque error. Therefore, using null voltage vectors only decreases torque, but there are better choices than this since the torque is always lower than its reference.

As shown in Fig. 7, the small and medium voltage vectors (V_{min} and V_{mid1}) replace the null voltage vectors in the segment of the 5-level torque hysteresis regulator (given by the red line), to increase the torque and reduce the steady state error of torque.

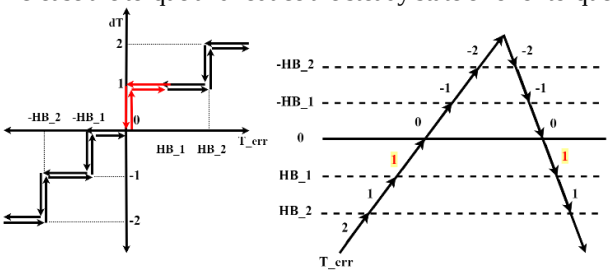

Fig. 7 –Modified 5-level torque hysteresis regulator.

As shown in Fig. 8, the selected voltage vector can increase or decrease the stator flux and the electromagnetic torque. For this, the choice of a group of voltage vectors in the first step depends on the requirement of torque variation. Therefore, if the torque error is in level 1, *i.e*., average torque response, the selected voltage vector grou contains small and medium vectors (V_{min} and V_{mid1}). If the torque error is in level 2, the torque controller output requires a fast response and high torque ripple, and the group contains medium and large vectors (V_{mid1} and V_{max}).

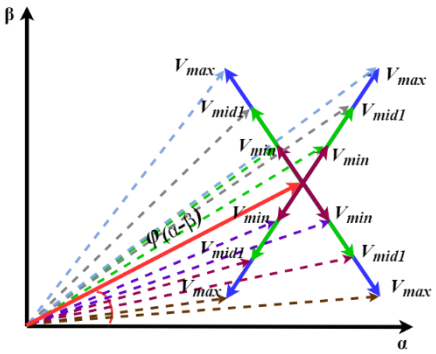

Fig. 8 – Effect of the different vectors on the variation of flux and torque.

To minimize the harmonic currents, the second step of the developed DTC depends greatly on the first step, which gives the selected group.

Table 2

Modified switching table

	Sector of the stator flux in (x-y) subspace											
Group	S_1	S_2	S_3	S_4	S_5	S_6	S_7	S_8	S_9	S_{10}	S_{11}	S_{12}
G_1	V_{57}						$V_{48\text{-}54}$					
G_2	$V_{25\text{-}56}$						V_{52}					
G_3	V_{24}				$V_{36\text{-}60}$						V_{24}	
G_4	$V_{28\text{-}26}$			V_{44}						$V_{28\text{-}26}$		
G_5	V_{30}		$V_{12\text{-}45}$						V_{30}			
G_6		V_{13}						$V_{14\text{-}22}$				
G_7	$V_{15\text{-}9}$						V_6					
G_8	V_{11}						$V_{7\text{-}38}$					

G_9	$V_{3\text{-}27}$	V_{39}	
G_{10}	V_{19}	$V_{35\text{-}37}$	V_{11}
G_{11}		V_{33}	$V_{51\text{-}18}$
G_{12}		$V_{49\text{-}41}$	V_{50}

Table 2 presents the modified switching table based on the applied different voltage vectors to minimize the stator flux in the subspace (*x*-*y*). For example, if group 1 of voltage vectors is selected and the torque regulator output is set to 2 ($\Delta T_e = 2$), the voltage vector V_{48} will be applied if the stator flux is in the sector (7-12) and the vector V_{57} for the remaining sectors.

The developed direct torque control based on the modified 5-level hysteresis regulator can reduce the torque ripples and minimize harmonic currents in the DSIM.

Moreover, the developed controller can slightly reduce the steady state torque error compared with the classical controllers.

5. IMPROVEMENT OF STEADY-STATE ERROR OF TORQUE FOR MODIFIED 5-LEVEL REGULATOR

The modified 5-level torque controller previously discussed cannot greatly minimize the torque error in the direct torque control. For this, the presented section deals with an improved PI controller associated with the modified 5-level to reduce the torque error in the dual star induction motor (DSIM) driving conditions.

Based on equations (1, 2, 3, and 6), the variation of the instantaneous torque is expressed as [26]:

$$\frac{dT_e}{dt} = \frac{1}{k_2}\left[-R_s T_e - \frac{3}{2}k_1 p\omega\left(\varphi_{r\alpha}\varphi_{s\alpha} - \varphi_{r\beta}\varphi_{s\beta}\right) + \frac{3}{2}k_1 p\left(\varphi_{r\alpha}V_{s\beta} + \varphi_{r\beta}V_{s\alpha}\right)\right]. \quad (10)$$

where:

$$k_1 = \frac{M}{L_r}, k_2 = \frac{L_s L_r - M^2}{L_r}.$$

The torque variation depends on the torque's instantaneous value, the rotation speed, and the subspace voltage vector (α-β).

In the modified 5-level hysteresis controller and according to the torque error, the voltage vectors at different controller levels cannot significantly minimize the torque error in DTC.

Figure 9 illustrates that the average torque value is varied and unstable around its reference in different speed ranges, especially at high speed.

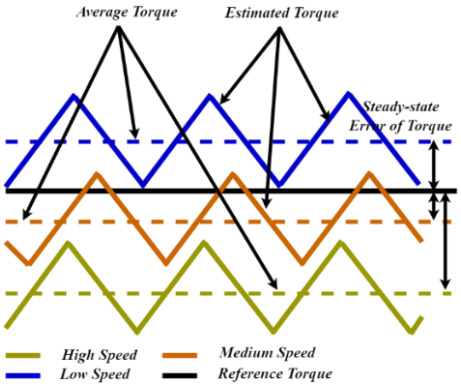

Fig. 9 – Torque waveform in different conditions.

For this aim, a PI controller can be incorporated with the modified 5-level to reduce the torque error under different driving conditions of the dual star induction motor (DSIM) (Fig. 10). The PI controller improves the accuracy of the modified 5-level hysteresis controller and therefore allows to reduce the torque error in steady state, which results in the following of the average torque value of its reference.

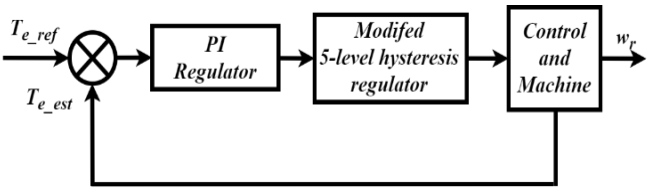

Fig. 10 – Control diagram of torque controller for DTC.

According to equation (10) and the non-linearity of the 5-level hysteresis controller, the proposed PI controller gains cannot be determined. Hence, the PI controller parameters should be selected to avoid large torque ripples. For this, once the PI controller parameters are well adjusted, the average torque value follows its reference, which implies that the torque error is reduced in a steady state. Moreover, the proposed PI controller cannot affect the performance of the DTC in terms of stator flux control and harmonic current minimization.

6. SIMULATION RESULTS

The simulation results were carried out using MATLAB/Simulink software. The DSIM, torque, and flux hysteresis bands for different DTC and PI regulator parameters are in the Appendix. In a steady state, the DSIM operates at a nominal speed of 1000 rpm, and with a load of 10 Nm, the flux reference is set to 1 Wb in all DTC techniques.

Figures 11 to 13 show the simulation results of the flux trajectory in the two subspaces (α-β) and (*x*-*y*) for conventional DTC based on 3-level hysteresis controller (3HL-DTC), DTC method based on 3-level hysteresis controller to minimize harmonic currents (3HL-MDTC) et DTC method based on 5-level hysteresis controller to minimize harmonic currents (5HL-DTC), respectively.

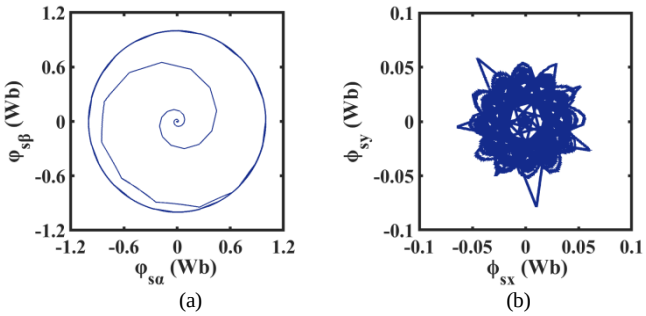

Fig. 11 –3HL-DTC technique: a) stator flux in (α-β) subspace; b)stator flux in (*x*-*y*) subspace.

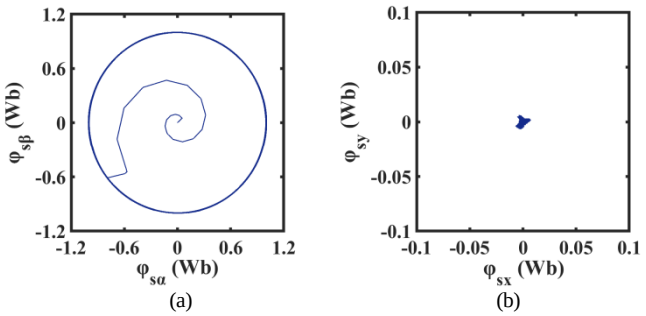

Fig. 12 –3HL-MDTC technique: a) stator flux in (α-β) subspace; b) stator flux in (*x*-*y*) subspace.

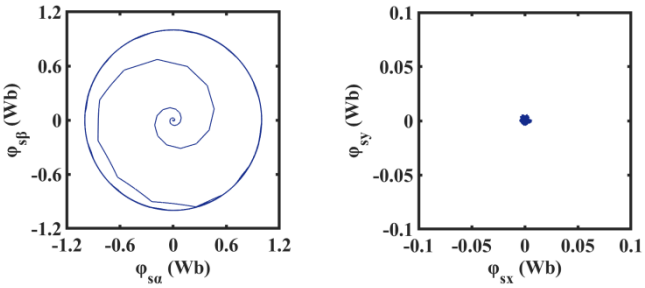

Fig. 13 –5HL-DTC technique; a) stator flux in (α-β) subspace: b) stator flux in (*x*-*y*) subspace.

The stator flux in the (α-β) subspace follows its reference in all three DTC techniques (Figs. 11–13a). Figure 11b shows that the stator flux in the (*x*-*y*) subspace is not controllable. Therefore, the 3HL-MDTC technique can reduce the stator flux in the (*x*-*y*) subspace (Fig. 12b). On the other hand, the appropriate voltage vectors of the 5HL-DTC technique have a similar effect as in the3HL-DTC technique to reduce the stator flux in the (*x*-*y*) subspace (Fig. 13b).

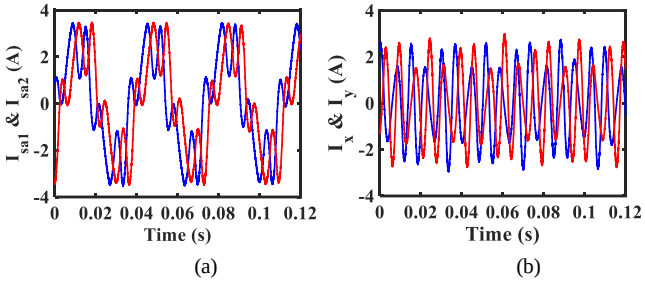

Fig. 14 –3HL-DTC technique: a) current of phase a1 and a2; b) current in (*x*-*y*) subspace.

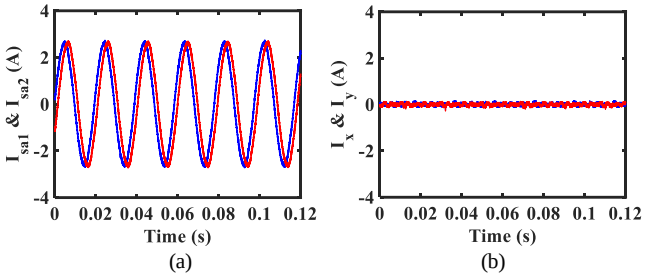

Fig. 15 –3HL-MDTC technique: a) current of phase a1 and a2; b) current in (*x*-*y*) subspace.

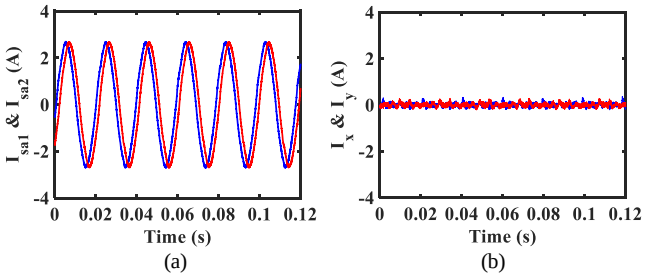

Fig. 16 –5HL-DTC technique: a) current of phase a1 and a2; b) current in (*x*-*y*) subspace.

As shown in Fig. 14, the 3HL-DTC suffers from the circulating current which the phase currents have a non-sinusoidal shape (Fig. 14a), caused by the large harmonic currents in the (*x*-*y*) subspace (Fig. 14b). Figure 15 shows that the modification of the switching table of the 3HL-DTC to build3HL-MDTC technique allows to minimize considerably the harmonic currents in the (*x*-*y*) subspace. As well as Fig. 16 shows that the 5HL-DTC technique presents an improved performance in terms of circulating current as in the 3HL-MDTC technique (Fig. 15). Moreover, in both techniques (3HL-MDTC and 5HL-DTC), the harmonic currents are reduced, and the current waveforms are much more sinusoidal.

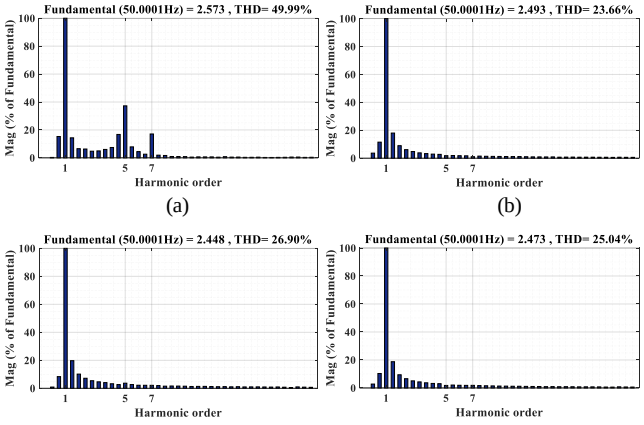

Fig. 17 – Phase current harmonic spectrum of different DTC techniques: a) 3HL-DTC; b) 3HL-MDTC; c) 5HL-DTC; d) 5HL-MDTC.

Figure 17 shows the FFT analysis of the phase a1 current for the 3HL-DTC, 3HL-MDTC, 5HL-DTC, and 5HL-MDTC techniques under the same conditions. It can be seen in Fig. 17a that the harmonic current components of orders 5 and 7 are essential in the 3HL-DTC technique caused by the circulating currents. According to Fig. 17b, the 3HL-MDTC technique can significantly reduce the fifth and seventh harmonic current. In contrast, the voltage vectors used in 3HL-DTC, 5HL-DTC, and 5HL-MDTC techniques can reduce the total harmonic distortion (THD) such as $THD_{3HL\text{-}DTC}$ = 49.99 %, $THD_{3HL\text{-}MDTC}$ = 23.66 %, $THD_{5HL\text{-}DTC}$ = 26.90 % and $THD_{5HL\text{-}MDTC}$ = 25.04 % (Figs. 17 b, c and d).

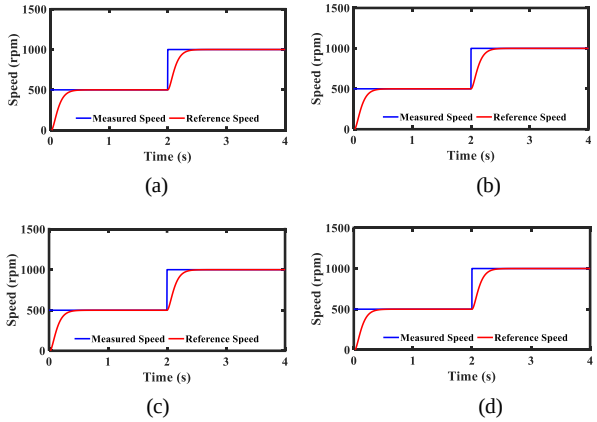

Fig. 18 –Dynamic speed response performance using different DTC techniques: a) 3HL-DTC; b) 3HL-MDTC; c) 5HL-DTC; d) 5HL-MDTC.

To check out the dynamic performance of the 3HL-DTC, 3HL-MDTC, 5HL-DTC, and 5HL-MDTC techniques, the references are given as follows: the load torque is set to10 Nm, and the speed varied from 500 rpm to 1000 rpm.

From Fig. 18, the rotor speed follows its references for 3HL-MDTC, 5HL-DTC, and 5HL-MDTC techniques, which implies that the modification on the hysteresis controllers and the voltage vectors chosen for the modified switching table gives good dynamic performance, such as in the 3HL-DTC technique.

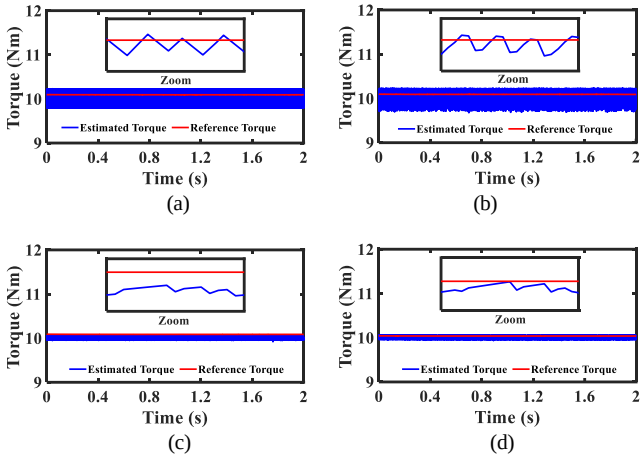

Fig. 19 – Steady-state performance of torque response in the different DTC techniques: a) 3HL-DTC; b) 3HL-MDTC; c) 5HL-DTC; d) 5HL-MDTC.

Figure 19 illustrates the response of the 3HL-DTC, 3HL-MDTC, 5HL-DTC, and 5HL-MDTC techniques regarding ripple and torque error in a steady state at a fixed rotor speed of 1000 rpm and a load of 10 Nm. The 3HL-DTC and the 3HL-MDTC techniques have significant ripples and high torque errors in the steady state (the average torque value does not follow its reference.

Figures 19 c, d illustrates that using the 5-level hysteresis controllers can significantly reduce the torque ripple compared to the 3HL-DTC and 3HL-DTC. Regarding Figs. 19 c, d 5HL-MDTC can minimize the steady-state torque error compared to 5HL-DTC, proving that replacing a zero voltage vector with a non-zero voltage vector gives an efficiency of the average torque value.

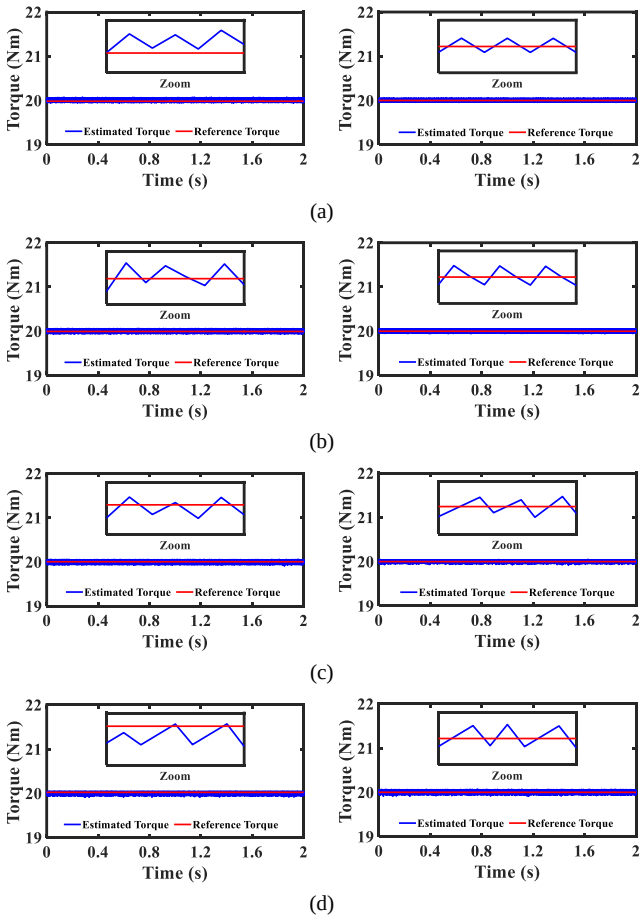

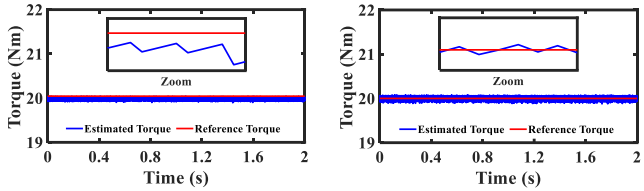

Fig. 20 – Steady-state performance of torque response left 5HL-MDTC technique and right proposed 5HL-PI-MDTC technique; a) 10 % rated speed; b) 25 % rated speed; c)50 % rated speed; d) 80 % rated speed; e) 100 % rated speed.

Figure 20 illustrates the DSIM response driven by the proposed DTC based on the modified 5-level hysteresis controller with PI controller to improve the steady-state torque error (5HL-PI-MDTC). Hence, a comparative study has been done between the proposed DTC and the 5HL-MDTC technique. For this, different reference speeds are varied from 10% to 100% of the rated speed with a load of 20 Nm. Figures 20 a, b, and c illustrate that the torque ripples are reduced at low and medium speeds compared to the 5HL-MDTC technique. However, in high speed, the (5HL-PI-MDTC) present less performance in term of torque ripples versus the 5HL-MDTC technique, but it presents significant results compared to the 3HL-DTC and 3HL-MDTC techniques (Figs. 20 d, e).

From Fig. 20, the 5HL-MDTC technique can significantly minimize the steady state torque error at low, medium, and high speeds. Consequently, the instantaneous average torque value follows its reference.

To perform the proposed control, an investigation of switching and core losses has been done for the DSIM drive. Hence, table 3 illustrates the switching losses in the 6-leg power inverter and the core losses of the DSIM drive for each method.

Table 3

Switching and core losses of the DSIM drive for each method

DTC methods	Switching Losses	Core losses
3HL-DTC	164,4 W	102.4025 W
3HL-MDTC	510.37 W	55.0665 W
5HL-DTC	378.96 W	59.7821 W
5HL-MDTC	395.14 W	58.6415 W
5HL-PI-DTC	332.99 W	57.6871 W

As shown by Table 3, the developed method based on a 5-level hysteresis controller presents less motor core losses compared to the other methods. Based on this analysis, the reduction of the stator flux harmonics and, therefore, the circulating current in subspace (*x*-*y*) leads to the reduction of the motor core losses for the entire torque-speed envelope typical for traction.

7. **CONCLUSION**

This paper has presented a modified direct torque control of dual star induction motor based on 3-level and 5-level hysteresis torque regulators to reduce harmonic currents, torque ripples, and steady-state torque error. The developed DTC techniques can significantly reduce the stator flux in the subspace (*x*-*y*), which presents the large harmonic components of the current that appear in the classical direct torque control based on the large voltage vectors.

Moreover, the 5-level hysteresis controller based on DTC applied the appropriate voltage vectors to reduce torque ripples. However, the 5-level hysteresis controller presents less performance in terms of steady-state error torque. To

reduce the error torque, a modified 5-level hysteresis controller has been developed based on the replacement of the zero-voltage vector by the active voltage vectors.

A PI controller has been incorporated into the modified 5-level hysteresis controller to improve the steady state response, which implies the instantaneous average torque value, referencing low, medium, and high speed.

This paper presents validation results to prove the effectiveness of the developed 5HL-PI-MDTC technique compared to the 3HL-MDTC, 5HL-DTC, and 5HL-MDTC techniques.

Received on 7 February 2023

APPENDIX

Table 4

2HL- DTC and3HL-DTCparameters

Parameters	Values
HB	±0.00025 Wb
HB	± 0.1 Nm

Table 5

Proposed 5HL-PI-MDTCparameters

Parameters	Values
K_p	0.1
K_i	50
HB_1	± 0.05 Nm
HB_2	± 0.1 Nm

Table 6

Machine parameters

Parameters	Values
Rated power	5.5 kW
Rated voltage	380 V
Rated current	6 A
Rated speed	1000 rpm
Number of poles	3
Rated Frequency	50 Hz
Stator resistance	2.03 Ω
Rotor resistance	3 Ω
Stator inductance	0.215 H
Rotor inductance	0.215 H
Mutual inductance	0.2 H
Moment of inertia	0.06 kg m^2
Coefficient of viscous friction	0.006 N m s/rad

REFERENCES

1. K. Marouani, K. Nounou, M. Benbouzid, B. Tabbache, *Investigation of energy-efficiency improvement in an electrical drive system based on multi-winding machines*, Electrical Engineering, **100**, pp. 205–216 (2016).
2. E. Levi, R. Bojoi, F. Profumo, H.A. Toliyat, S. Williamson, *Multiphase induction motor drives–a technology status review*, IET Electric Power Applications, **1**, *4*, pp. 489–516 (2007).
3. Y. Zhao, T.A. Lipo, *Space vector PWM control of dual three-phase induction machine using vector space decomposition*, IEEE Transactions on Industry Applications, **31**, *5*, pp. 1100–1109 (1995).
4. E. Levi, *Multiphase electric machines for variable-speed applications*, IEEE Transactions on Industrial Electronics, **55**, *5*, pp. 1893–1909 (2008).
5. R. Bojoi, M. Lazzari, F. Profumo, A. Tenconi, *Digital field-oriented control for dual three-phase induction motor drives*, IEEE Transactions on Industry Applications, **39**, *3*, pp. 752–760 (2003).
6. K. Iffouzar, M.F. Benkhoris, H. Aouzellag, K. Ghedamsi, D. Aouzellag, *Direct rotor field-oriented control of polyphase induction machine based on fuzzy logic controller*, Rev. Roum. Sci. Techn. – Électrotechn. et Énerg., **62**, *1*, pp. 42–47 (2017).
7. K. Iffouzar, M.F. Benkhoris, K. Ghedamsi, D. Aouzellag, *Behavior analysis of a dual stars induction motor supplied by pwm multilevel inverters*, Rev. Roum. Sci. Techn. – Électrotechn. et Énerg., **61**, *2*, pp. 137–141 (2016).
8. L. Youb, A. Crăciunescu, *Direct torque control and vectorial control of the induction motor*, Rev. Roum. Sci. Techn. – Électrotechn. et Énerg., **53**, *1*, pp. 87–98 (2008).
9. R.M. Ariff, D. Hanafi, W.M. Utomo, N.M. Zin, S.Y. Sim, A.A. Bohari, *Takagi-Sugeno fuzzy purpose as speed controller in indirect field-oriented control of induction motor drive*, International Journal of Power Electronics and Drive Systems, **8**, *2*, pp. 513–521 (2017).
10. S. Sit, H.R. Ozcalik, E. Kilic, *An efficient speed control method based on neuro-fuzzy modeling for asynchronous motors*, Rev. Roum. Sci. Techn. – Électrotechn. et Énerg., **63**, *3*, pp. 326–331 (2018).
11. I. Takahashi, T. Noguchi, *A new quick-response and high-efficiency control strategy of an induction motor*, IEEE Transactions on Industry Applications, **IA-22**, *5*, pp. 820–827 (1986).
12. A. Idir, M. Kidouche, *Rt-lab and dspace: two softwares for real time control of induction motors*, Rev. Roum. Sci. Techn. – Électrotechn. et Énerg., **59**, *2*, pp. 205–214 (2014).
13. A. Azib, D. Ziane, T. Rekioua, A. Tounzi, *Robustness of the direct torque control of double star induction motor in fault condition*, Rev. Roum. Sci. Techn. – Électrotechn. et Énerg., **61**, *2*, pp. 147–152 (2016).
14. K. Hatua, V.T. Ranganathan, *Direct torque control schemes for split-phase induction machine*, IEEE Transactions on Industry Applications, **41**, *5*, pp. 1243–1254 (2005).
15. R. Bojoi, F. Farina, G. Profumo, A. Tenconi, *Direct torque control for dual three-phase induction motor drives*, IEEE Transactions on Industry Applications, **41**, *6*, pp. 433–448 (2016).
16. H. Lallouani, B. Saad, *Performances of type 2 fuzzy logic control based on direct torque control for double star induction machine*, Rev. Roum. Sci. Techn. – Électrotechn. et Énerg., **65**, *1-2*, pp. 103–108 (2020).
17. K. Gopakumar, V.T. Ranganthan, S.R. Bhat, *Split-phase induction motor operation from PWM voltage source inverter*, IEEE Transactions on Industry Applications, **29**, *5*, pp. 927–932 (1993).
18. M.A. Abbas, R. Christen, T.M. Jahns, *Six-phase voltage source inverter driven induction motor*, IEEE Transactions on Industrial Application, **IA-20**, *5*, pp. 1251–1259 (1984).
19. D. Hadiouche, L. Baghli, A. Rezzoug, *Space-vector PWM techniques for dual three-phase AC machine: analysis, performance evaluation, and DSP implementation*, IEEE Transactions on Industry Applications, **42**, *4*, pp. 1112–1122 (2006).
20. E. Levi, *Advances in converter control and innovative exploitation of additional degrees of freedom for multiphase machines*, IEEE Transactions on Industrial Electronics, **63**, *1*, pp. 433–448 (2016).
21. M. Duran, F. Barrero, *Recent advances in the design, modeling, and control of multiphase machines part II*, IEEE Transactions on Industrial Electronics, **63**, *1*, pp. 459–468 (2016).
22. L.B. Zheng, J.E. Fletcher, B.W. Williams, X.N. He, *A novel direct torque control scheme for a sensorless five-phase induction motor drive*, IEEE Transactions on Industrial Electronics, **58**, *2*, pp. 503–513 (2011).
23. G. Abad, M. Á. Rodríguez, J. Poza, *Two-level VSC based predictive direct torque control of the doubly fed induction machine with reduced torque and flux ripples at low constant switching frequency*, IEEE Transactions on Power Electronics, **23**, *3*, pp. 1050–1061 (2008).
24. Y. Zhang, J. Zhu, *A novel duty cycle control strategy to reduce both torque and flux ripples for DTC of permanent magnet synchronous motor drives with switching frequency reduction*, IEEE Transactions on Power Electronics, **26**, *10*, pp. 3055–3055 (2011).
25. Y. Zhang, J. Zhu, *Direct torque control of permanent magnet synchronous motor with reduced torque ripple and commutation frequency*, IEEE Transactions on Power Electronics, **26**, *1*, pp. 235–248 (2010).
26. Y. Tatte, *Torque ripple minimization with modified comparator in DTC based three-level five-phase inverter fed five-phase induction motor*, IET Power Electronics, **14**, *9*, pp. 1713–1723 (2021).
27. Y.N. Tatte, M.V. Aware, J.K. Pandit, R. Nemade, *Performance improvement of three-level five-phase inverter-fed DTC-controlled five-phase induction motor during low-speed operation*, IEEE Transactions on Industry Applications, **54**, *3*, pp. 2349–2357 (2018).
28. A. Wang, H. Zhang, J. Jiang, D. Jin, S. Zhu, *Predictive direct torque control of permanent magnet synchronous motors using deadbeat torque and flux control*, Journal of Power Electronics, **23**, *2*, pp. 264–273 (2023).
29. F. Yang, H. Chen, V. Pires, J. Martins, Y. Gorbounov, X. Li, M. Orabi, *Improved direct torque control strategy for reducing torque ripple in switched reluctance motors*, Journal of Power Electronics, **22**, *4*, pp. 603–613 (2022).
30. S.S. Hakami, K.B. Lee, *Four-level hysteresis-based DTC for torque capability improvement of IPMSM fed by three-level NPC inverter*, Electronics, **9**, *10*, 1558 (2020).
31. H. Masoumkhani, A. Taheri, *PI regulator-based duty cycle control to reduce torque and flux ripples in DTC of six-phase induction*

motor, IEEE Transactions on Power Electronics, **9**, *1*, pp. 354–370 (2018).

32. Y.N. Tatte, M.V. Aware, *Direct torque control of five-phase induction motor with common-mode voltage and current harmonics reduction*, IEEE Transactions on Power Electronics, **32**, *11*, pp. 8644–8654 (2016).
33. Y. Ren, Z.Q. Zhu, *Reduction of both harmonic current and torque ripple for dual three-phase permanent-magnet synchronous machine using modified switching-table-based direct torque control*, IEEE Transactions on Industrial Electronics, **62**, *11*, pp. 6671–6683 (2015).
34. Y. Gao, L. Parsa, *Modified direct torque control of five-phase permanent magnet synchronous motor drives*, IEEE Applied Power Electronics Twenty Second Annual Conference, pp. 1428–1433 (2007).
35. K.D. Hoang, Y. Ren, Z.Q. Zhu, M. Foster, *Modified switching-table strategy for reduction of current harmonics in direct torque controlled dual-three-phase permanent magnet synchronous machine drives*, IET Electric Power Applications, **9**, *1*, pp. 10–19 (2015).
36. K.D. Hoang, Z.Q. Zhu, M. Foster, *Optimum look-up table for reduction of current harmonics in direct torque controlled dual three-phase permanent magnet brushless ac machine drives*, Sixth IET International Conference on Power Electronics, Machines and Drives, pp. 1–6 (2012).
37. J. Xu, M. Odavic, Z.Q. Zhu, Z.Y. Wu, N. Freire, *Switching-table-based direct torque control of dual three-phase PMSMs with closed-loop current harmonics compensation*, IEEE Transactions on Power Electronics, **36**, *9*, pp. 10645–10659 (2021).